Supporting information

Suitable Energy Avenue For Dimension-Matched Cascade Charge Transfer Mechanism in g-C_3N_4/TS-1 Heterostructure Co-Doped With Au-TiO_2 For Artificial Photosynthetic Green Fuel Production

Imran Khan [a,b], Salman Khan [c], Amir Zada [*] [d], Ahmad Ismail [c], Sharafat Ali [e], Muhammad Ishaq Ali Shah [d], Muhammad Ateeq [d], Perveen Fazil [f], Javed Ali Khan [d], Afsar Khan [g], Farooq Jan [h], Dilawar Farhan Shams [i], Baoji Miao [b], Shiliang Wang [a,*]*

[a] *School of Physics and Electronics, Central South University, 410083, Changsha, People's Republic of China*

[b] *Henan International Joint Laboratory of Nano-Photoelectric Magnetic Materials. School of Materials Science and Engineering, Henan university of Technology. Zhengzhou city,450001*

[c] *Key Laboratory of Functional Inorganic Materials Chemistry (Heilongjiang University), Ministry of Education, School of Chemistry and Materials Science, International Joint Research Center and Lab for Catalytic Technology, Harbin 150080, PR China.*

[d] *Department of Chemistry, Abdul Wali Khan University, Mardan, Khyber Pakhtunkhwa, 23200, Pakistan*

[e] *School of Physics, University of Electronic Science and Technology of China, Chengdu 610054, China*

[f] *Department of Chemistry, University of Karachi, Karachi, 75270, Pakistan*

[g] *School of Mineral Processing and Bioengineering, Central South University, 410083, Changsha, People's Republic of China*

[h] *Department of Botany, Abdul Wali Khan University, Mardan, Khyber Pakhtunkhwa, 23200, Pakistan*

[i] *Department of Environmental Sciences, Abdul Wali Khan University, Mardan, Khyber Pakhtunkhwa, 23200, Pakistan*

Corresponding author: Shiliang Wang (shiliang@csu.edu.cn) and Amir Zada (amistry009@yahoo.com)

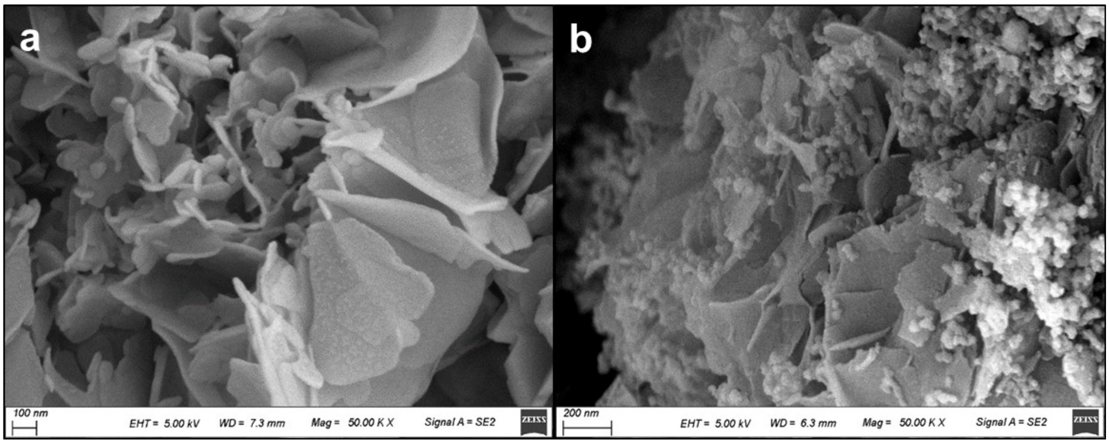

Figure S1. SEM image of TS nanosheets and (8CN/0.7M/TS).

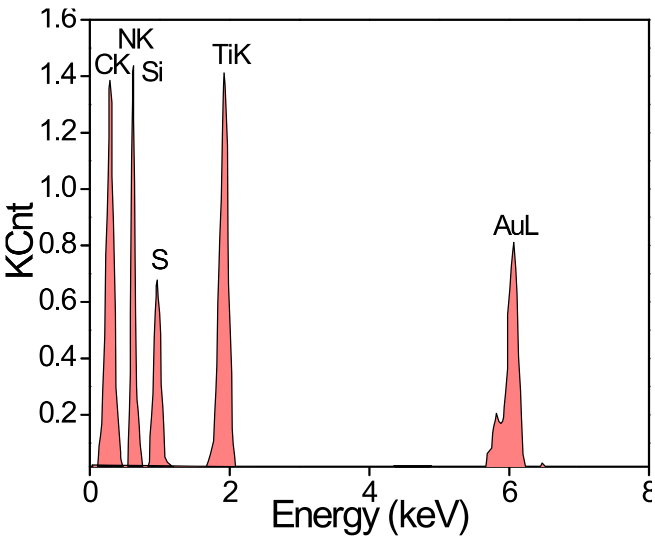

Figure S2. EDX analysis of 1Au-4T/8CN/0.7hTS nanocomposites.

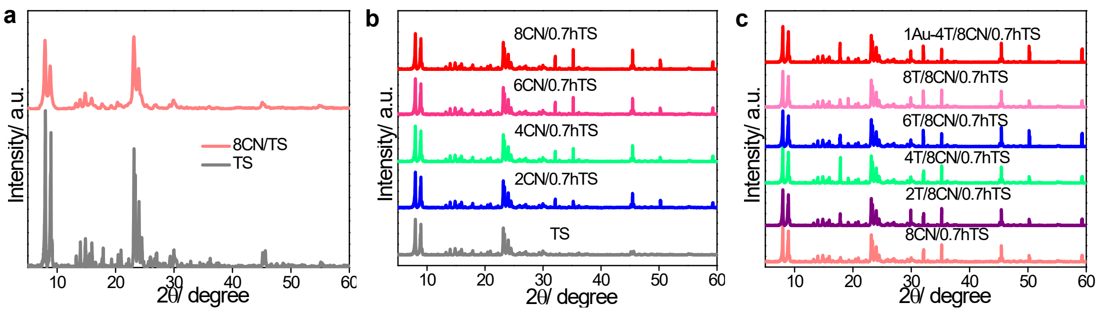

Figure S3. XRD patterns of TS and 8CN/TS a), 8CN/TS, 8CN/0.3hTS, 8CN/0.5hTS, 8CN/0.7hTS and 8CN/1hTS b). and c), XRD patterns of 8CN/0.7hTS, 2T/8CN/0.7hTS, 4T/8CN/0.7hTS, 6T/8CN/0.7hTS, 8T/8CN/0.7hTS and 1Au-4T/8CN/0.7hTS.

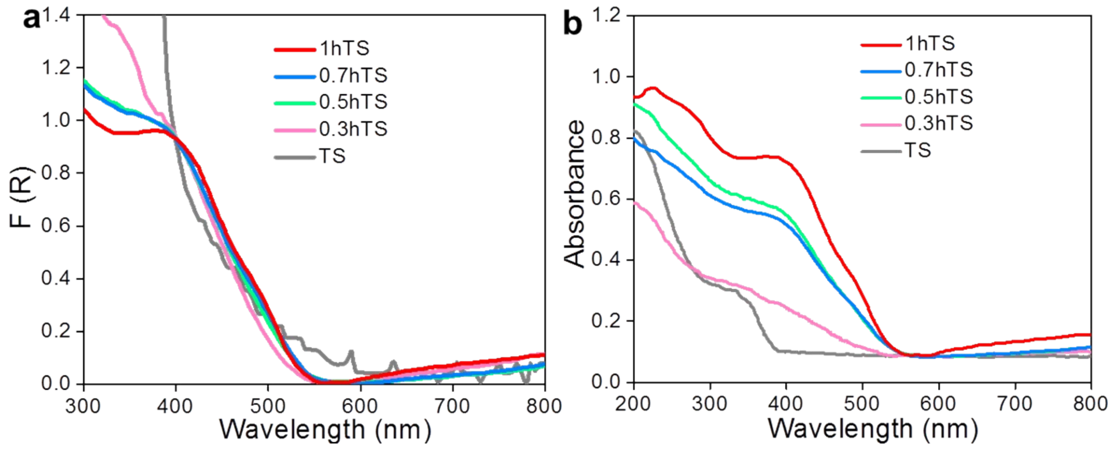

Figure S4. UV-vis diffuse reflectance spectra a) and b), and energy band gaps of different sulphated Mn modified samples c). The labels 0 #, 0.3 #, 0.5#, 0.7 # and 1 # denote samples in which the wt.% sulfur (S) was 0%, 1%, 5%, 7%, and 10%, respectively.

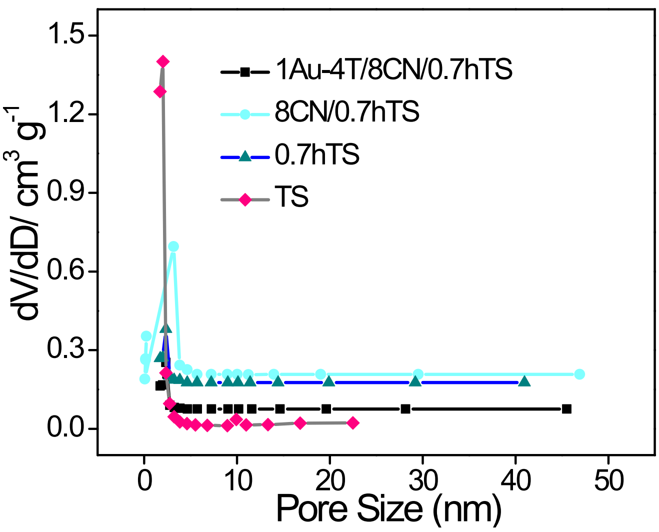

Figure S5. N_2 adsorption/desorption isotherm curves and pore diameter of TS, 0.7hTS, 8CN/0.7hTS, and 1Au-4T/8CN/0.7hTS.

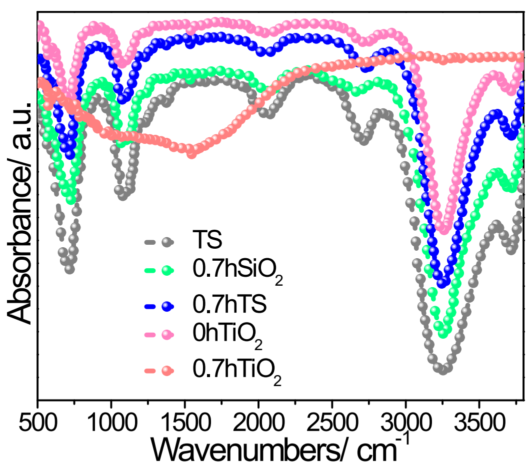

Figure S6. FTIR spectra of different samples.

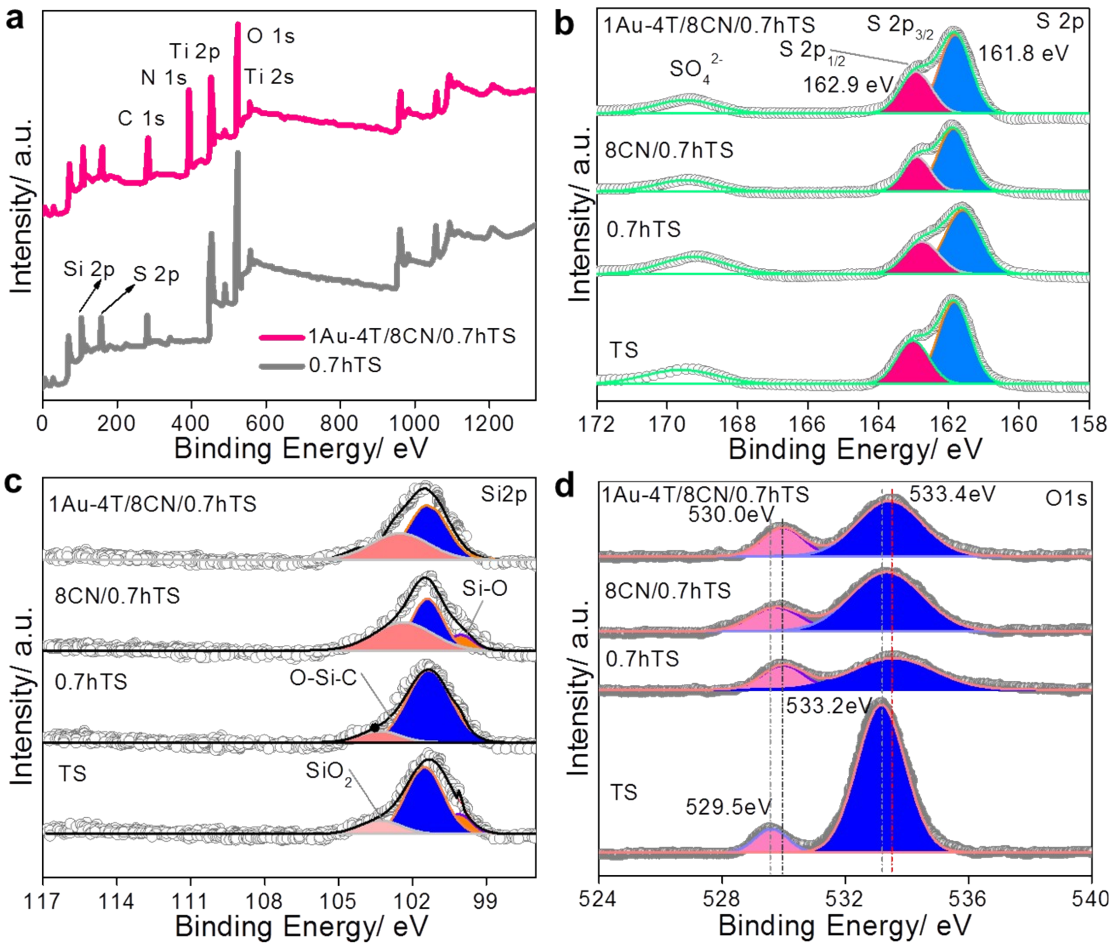

Figure S7. XPS survey spectra a), XPS survey spectra of S2p b), Si2p c), and O1s d), of TS, 0.7hTS, 8CN/0.7hTS, 4T/8CN/0.7hTS and 1Au-4T/8CN/0.7hTS samples.

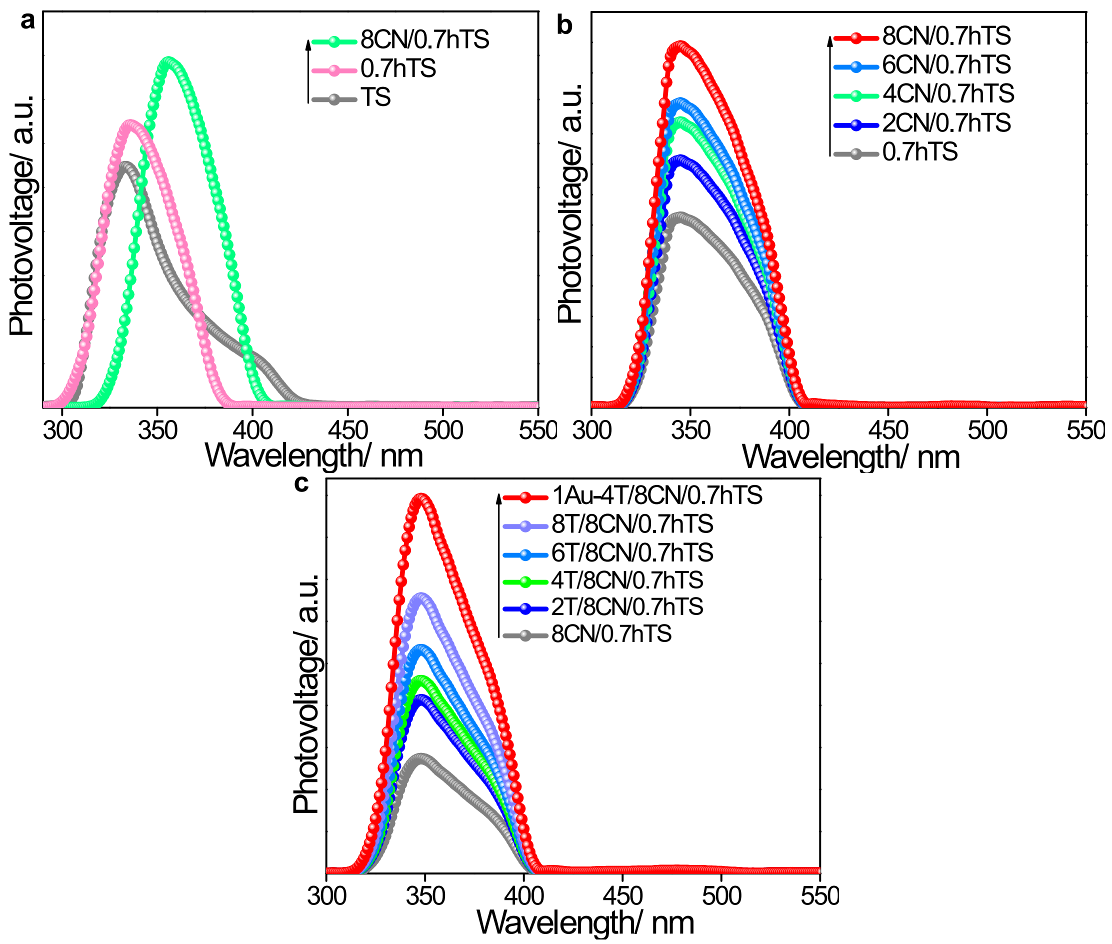

Figure S8. SS-SPS spectra of TS, 0.7hTS and 8CN/0.7hTS a), 8CN/0.3hTS, 8CN/0.5hTS, 8CN/0.7hTS, 8CN/1hTS b), and 8CN/0.7hTS, 2T/8CN/0.5hTS, 4T/8CN/0.5hTS, 6T/8CN/0.5hTS, 8T/8CN/0.7hTS and 1Au-4T/8CN/0.7hTS c).

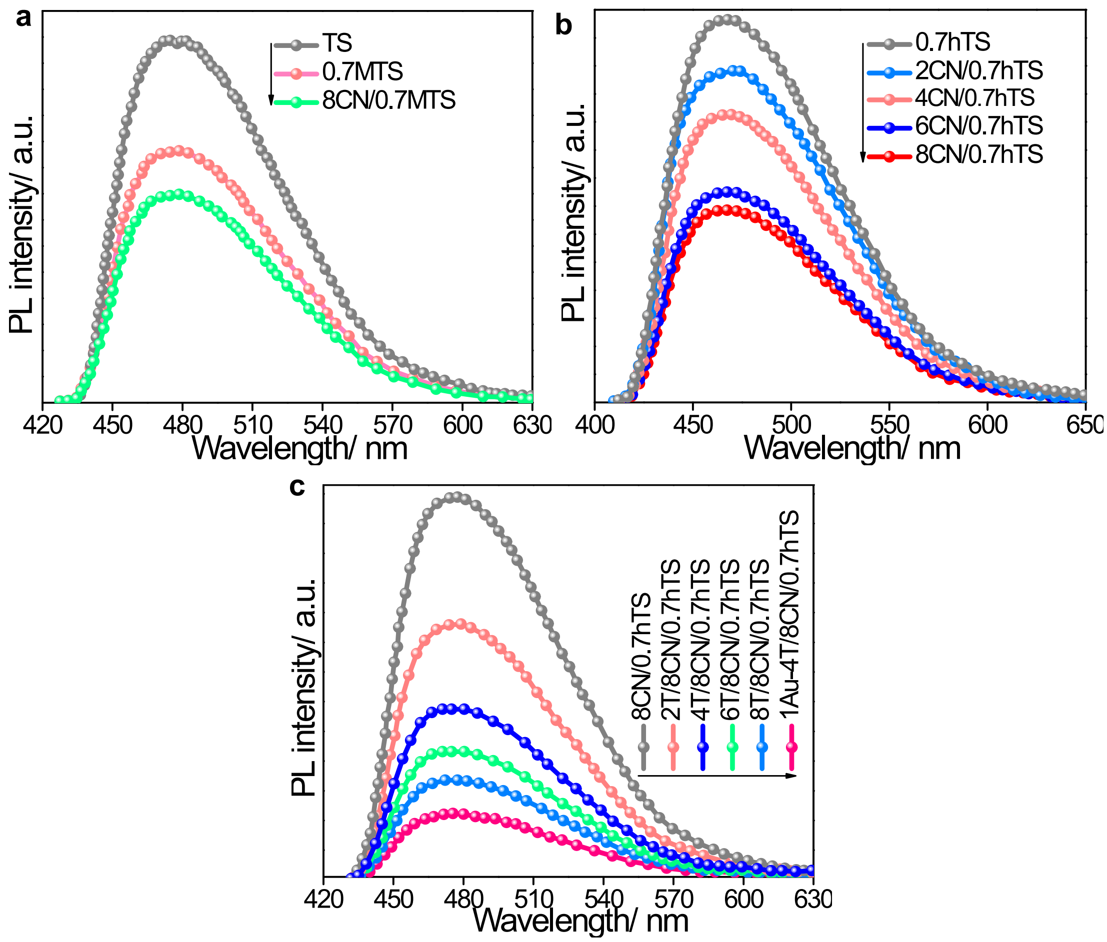

Figure S9. Photoluminescence spectra of TS, 0.7hTS and 8CN/0.7hTS a), 0.7hTS, 8CN/0.3hTS, 8CN/0.5hTS, 8CN/0.7hTS and 8CN/1hTS b) and 2T/8CN/0.7hTS, 4T/8CN/0.7hTS, 6T/8CN/0.7hTS, 8T/8CN/0.7hTS) and 1Au-4T/8CN/0.7hTS c).

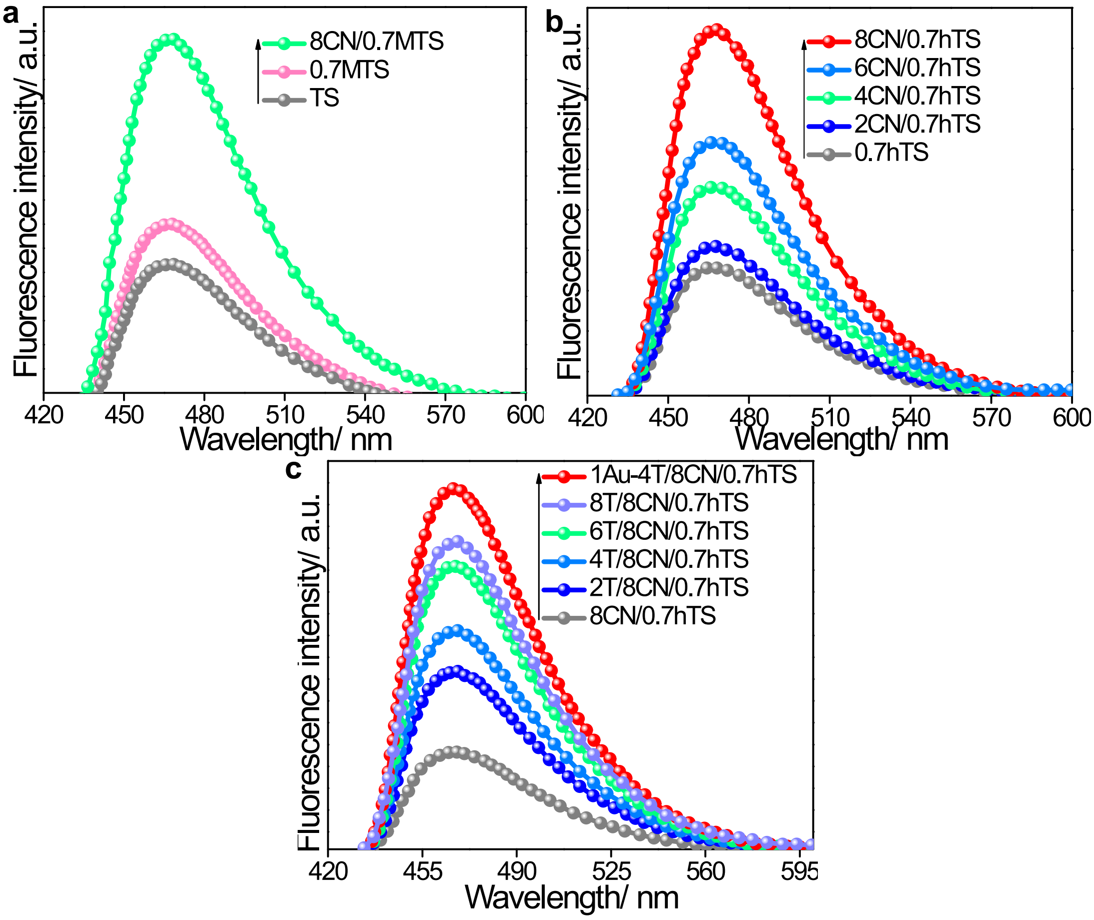

Figure S10. Fluorescence spectra related to the produced hydroxyl radical amounts of TS, 0.7hTS and 8CN/0.7hTS a), 0.7hTS, 8CN/0.3hTS, 8CN/0.5hTS, 8CN/0.7hTS and 8CN/1hTS b) and 2T/8CN/0.7hTS, 4T/8CN/0.7hTS, 6T/8CN/0.7hTS, 8T/8CN/0.7hTS and 1Au-4T/8CN/0.7hTS c).

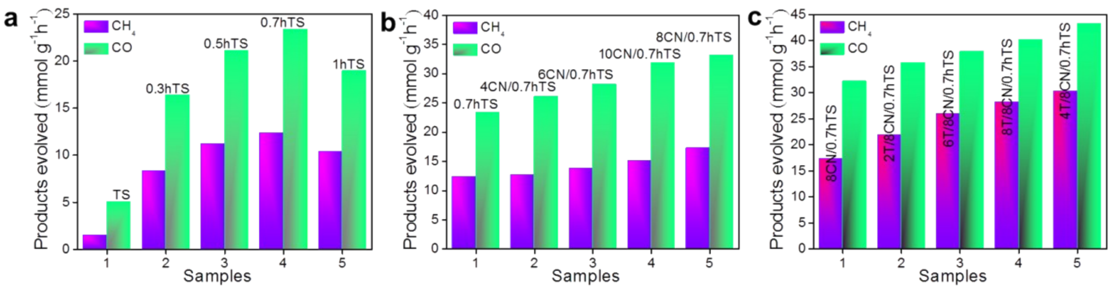

Figure S11. Visible-light photocatalytic activities for CO_2 conversion of TS, 0.3hTS, 0.5hTS, 0.7hTS and 1hTS a) and 2CN/0.7hTS, 4CN/0.7hTS, 6CN/0.7hTS, 8CN/0.7hTS and 10CN/0.7hTS b), and 2T/8CN/0.7hTS, 4T/8CN/0.7MTS), 6T/8CN/0.7hTS, 8T(8CN/0.7hTS) and 1Au-4T/8CN/0.7hTS c).

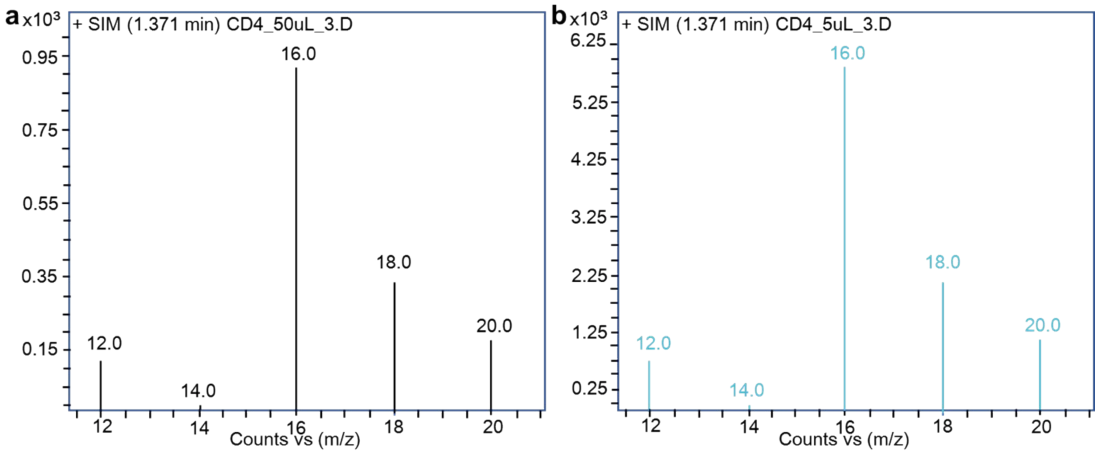

Figure S12. The GC-Mass analysis of photocatalytic reduction products of CO_2 on 1Au-4T/8CN/0.7hTS after irradiation for 6h without methanol a) and with methanol b).

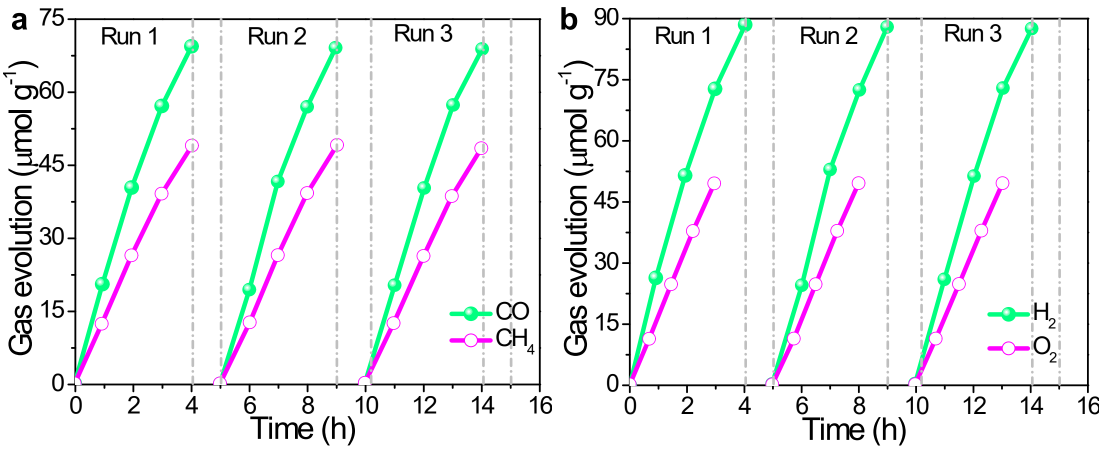

Figure S13. Three consecutive runs of CO_2 reduction by 1Au-4T/8CN/0.7hTS under visible-light irradiation.

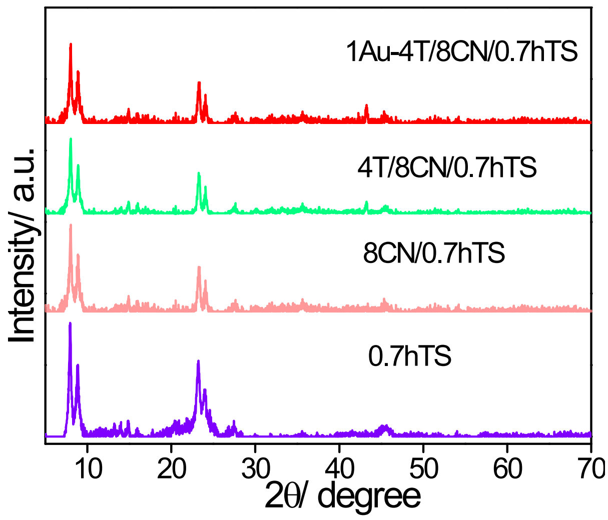

Figure S14. XRD patterns of 0.7hTS, 8CN/6T/0.7hTS, 4T/8CN/0.7hTS and 1Au-4T/8CN/0.7hTS after long term stability test.

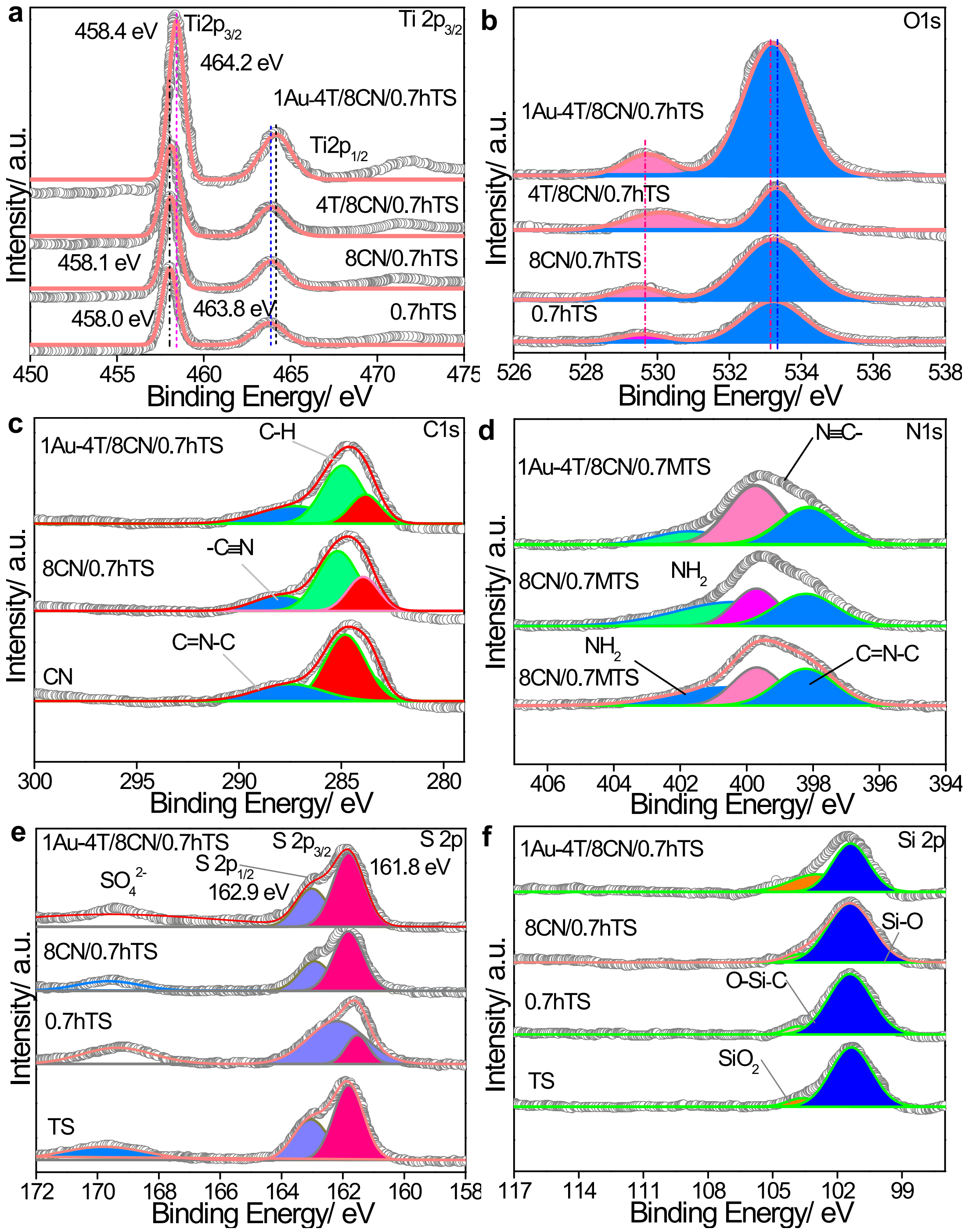

Figure S15. XPS survey spectra of Ti $2p_{3/2}$ a), XPS survey spectra of O1s b), C 1s c), and N 1s d), S 2p e) and f), Si 2p of TS, 0.7hTS, 8CN/0.7hTS, and 1Au-4T/8CN/0.7hTS samples after long term stability test.

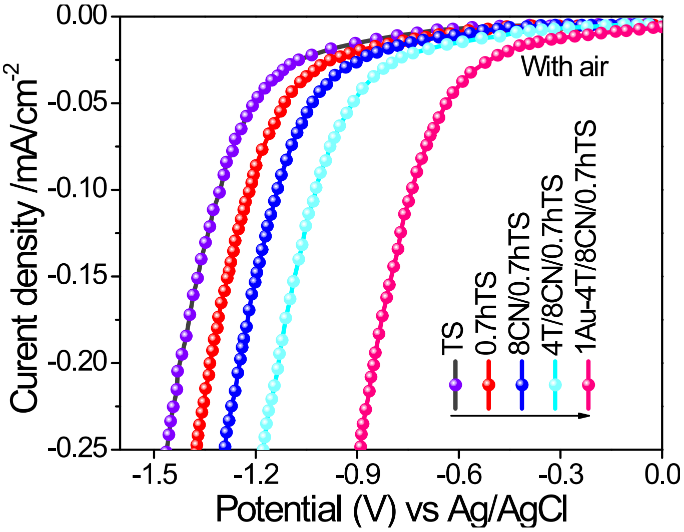

Figure S16. Electrochemical reduction curves in the air-bubbled system of TS, 0.7hTS, 0.7hTS, 8CN/6T/0.7hTS, 4T/8CN/0.7hTS and 1Au-4T/8CN/0.7hTS. Electrochemical performance was measured in a 0.5 M Na_2SO_4 solution, and Hg/Hg_2Cl_2 (saturated KCl) electrode was used as the reference electrode.

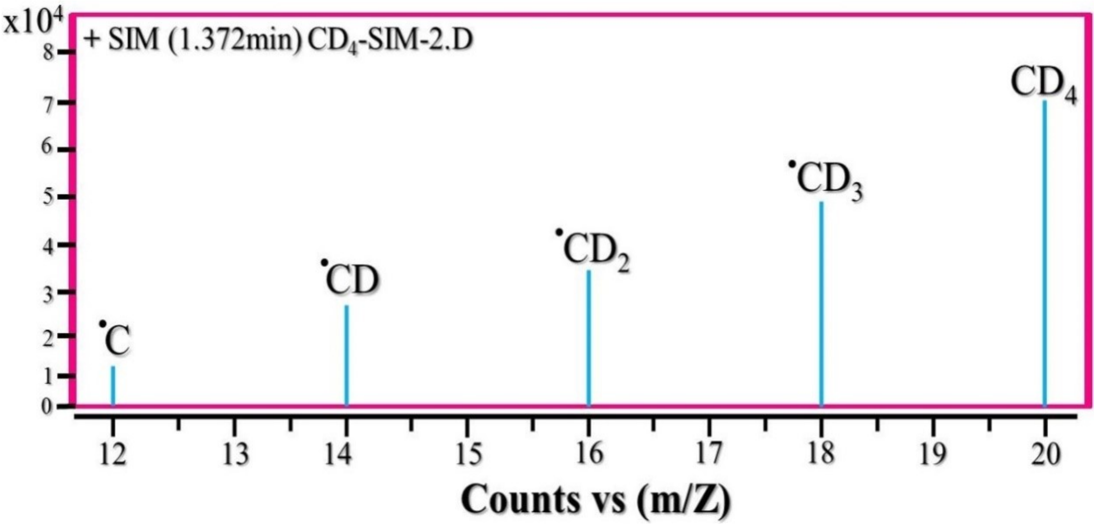

Figure S17. GC-Mass Spectrometry analyses of intermediate products after visible-light photocatalytic conversion of CO_2 over 1Au-4T/8CN/0.7hTS photocatalyst for 8h. The identified intermediate products, including CD (m/z=14), CD_2 (m/z=16), CD_3 (m/z=18), and CD_4 (m/z=20) are labeled in the figure.

Table S1. C, N, Ti, S, Au contents (mol%) in TS, 0.7hTS, 8CN/0.7hTS, and 1Au-4T/8CN/0.7hTS according to elemental analysis.

Samples	N	C	Ti	S	Au
TS	0	0	13.45	1.8	0
0.7hTS	0	0	13.12	1.82	0
8CN/0.7hTS	23.14	25.34	12.36	1.76	0
4T/8CN/0.7hTS	22.65	26.06	11.16	1.8	0
1Au-4T/8CN/0.7hTS	23.12	25.55	13.31	1.7	0.45
Elemental ICP analysis after long term CO_2 reduction reaction:					
TS	0	0	13.25	1.6	0
0.7hTS	0	0	13.12	1.72	0
8CN/0.7hTS	22.17	24.31	11.48	1.79	0
4T/8CN/0.7hTS	22.87	25.00	12.09	1.75	0
1Au-4T/8CN/0.7hTS	22.79	25.35	13.21	1.66	0.45